Theoret. Comput. Fluid Dynamics (2001) 15: 143–163

Theoretical and Computational Fluid Dynamics

© Springer-Verlag 2001

Wall Effect on the Convective–Absolute Boundary for the Compressible Shear Layer

Jean-Christophe Robinet* **and Jean-Paul Dussauge**

Institut Universitaire des Systèmes Thermiques Industriels, UMR 6595,
CNRS Université de Provence (Aix-Marseille I), Centre de St Charles,
12 avenue Général Leclerc, 13003 Marseille, France
robinet@paris.ensam.fr, dussauge@iusti.univ-mrs.fr

Grégoire Casalis

Department of Modelling Aerodynamics and Energetics, ONERA-Toulouse,
2 avenue Edouard Belin, 31055 Toulouse Cedex 4, France
casalis@onecert.fr

Communicated by M. Y. Hussaini

Received 9 May 2001 and accepted 21 August 2001

Abstract. The linear stability of inviscid compressible shear layers is studied. When the layer develops at the vicinity of a wall, the two parallel flows can have a velocity of the same sign or of opposite signs. This situation is examined in order to obtain first hints on the stability of separated flows in the compressible regime. The shear layer is described by a hyperbolic tangent profile for the velocity component and the Crocco relation for the temperature profile. Gravity effects and the superficial tension are neglected. By examining the temporal growth rate at the saddle point in the wave-number space, the flow is characterized as being either absolutely unstable or convectively unstable. This study principally shows the effect of the wall on the convective–absolute transition in compressible shear flow. Results are presented, showing the amount of the backflow necessary to have this type of transition for a range of primary flow Mach numbers M_1 up to 3.0. The boundary of the convective–absolute transition is defined as a function of the velocity ratio, the temperature ratio and the Mach number. Unstable solutions are calculated for both streamwise and oblique disturbances in the shear layer.

1. Introduction

An understanding of the stability of compressible shear layers is of fundamental interest and is also important for pratical problems found in hypersonic propulsion, as the mixing in scramjets. In particular, the shear layer can be regarded as a simple model of the injection device of fuel into an air system. The prediction and the control of such a flow necessitates knowing their characteristics and in particular the nature of the instability waves (convective or absolute), which can develop in a shear layer. Linear stability analysis has been used extensively in examining free or confined compressible shear layers. Pioneering work on stability theory of compressible shear flows, both free and wall bounded, is due to Lee and Lin (1946) and Dunn

* *Present address:* SINUMEF, ENSAM, 151 Bd. de l'Hopital, 75013 Paris, France.

and Lin (1955), who first showed the importance of three-dimensional disturbances for the stability of these flows. Lessen *et al.* (1965, 1966) Blumen *et al.* (1975), Tam and Morris (1980), Jackson and Grosch (1989, 1990a,b, 1991a,b) and others have demonstrated that the Kelvin–Helmholtz instability, which was the main instability of the shear layers, became less and less amplified as the convective Mach number increased. Jackson and Grosch (1989) have shown that when the Mach number increased, the subsonic modes are transformed into supersonic modes which are subsonic at one boundary and supersonic at the other. Jackson and Grosch (1989) have shown that there was an infinite set of discrete modes, of which the first is a vortical mode and all the others are acoustic modes. They have also shown that three-dimensional disturbances have the same general characteristics as two-dimensional disturbances. On the other hand, a decrease in the temperature ratio $S = T_2/T_1$, where the upstream quantities are denoted by the subscript 1 and the downstream ones by the subscript 2, results in an increase for the growth rate of the unstable waves at any Mach number. Finally, Jackson and Grosch (1991a) have shown that the characteristic features of the solutions to the stability problem for the compressible shear layer are qualitatively similar for a large range of thermodynamic models. Nevertheless, in all these studies, the shear layers were assumed to be free and unconfined. In the case of supersonic shear layers inside a rectangular channel, such as those in a ramjet combustor, see Tam and Hu (1989), Mack (1989), Greenough *et al.* (1989), Zhuang *et al.* (1989), Jackson and Grosch (1990a) and Gathmann *et al.* (1993), the situation is quite different. The unsteady motion of the shear layer is invariably coupled to the acoustic modes of the rectangular channel through reflections of the acoustic waves by the channel walls. Tam and Hu (1989) have found that two-dimensional supersonic shear layers inside a rectangular channel may undergo supersonic instabilities. These supersonic instability waves are generated by Mach wave systems formed by reflections from the channel walls. They exist only when the convective Mach numbers of the flow on both sides of the shear layer are supersonic.

Nevertheless, in all of these studies, the type of instability is classified from either its spatial or temporal growth, depending on whether the frequency is real and the wave number complex or vice versa. These classifications are quite arbitrary unless one examines carefully the propagative character (i.e., the group velocity) of the instability waves. The work of Huerre and Monkewitz (1985) addressed this point and emphasized the important distinction between absolute and convective instability in the context of shear flow. A flow is said to be absolutely unstable if the response to an impulse in space and time is unbounded everywhere in space for large value of the time. A flow is said to be convectively unstable if the response decays to zero in the reference frame for large time. Huerre and Monkewitz (1985) have pointed out that an occurrence of a saddle point in the number wave space may be related to a transition from convective to absolute instability. If such a transition occurs, the spatial stability theory is no longer appropriate and temporal calculations are now required. Huerre and Monkewitz (1985) have shown that the incompressible shear layer is convectively unstable for $R = U_2/U_1 > 0$. In fact, they have shown that the shear layer became absolutely unstable only if the low-speed stream had an ambient speed, say U_2, which was less than $-0.136U_1$, where U_1 is the speed of the high-speed stream. That is, there must be a sufficiently large counterflow before the incompressible shear layer becomes absolutely unstable and a temporal stability theory becomes relevant. The distinction between absolutely or convectively unstable flows, which derives from consideration of the impulse response of the flow, is clearly dependent upon the frame of reference. However, in all laboratory contexts the reference frame is fixed and no ambiguity exists. Furthermore, these concepts become particularly significant in nonparallel flows where the propagative character of the instability may change locally as the flow develops in the streamwise direction and, consequently, another intrinsic length scale (the streamwise length scale over which the flow is absolutely unstable) should be introduced, which can have an important dynamical role in determining the response of the flow. In some particular conditions, this can lead to a strong frequency selection mechanism and force a long-range spatial order to the flow. The convective–absolute classification of an instability is also an important issue in regard to flow control. Localized forcing of a flow in order to influence its space–time development will be effective, perhaps, only if the flow is convectively unstable. In an absolutely unstable flow the forcing will be rapidly overwhelmed by the *in situ* growing instability. For this reason, it is useful to define the parameter ranges wherein a flow is either absolutely or convectively unstable. Nevertheless, the convective–absolute transition in the shear layer in a three-dimensional compressible fluid has not been studied as extensively as in an incompressible fluid. Independently, Pavithran and Redekopp (1989) and Jackson and Grosch (1990b) have studied the transition from convective to absolute instability in a compressible, subsonic two-dimensional, free shear layer. They found that as the Mach number increased in the subsonic

regime, so did the amount of backflow necessary to go from convective to absolute instability. They also found that when the slow stream was cooled with respect to the high-speed stream at a fixed Mach number, the amount of backflow necessary to go from convective to absolute instability decreased. However, their studies are limited to the subsonic regime and for two-dimensional waves. To our knowledge, there are no studies dealing with the convective–absolute transition of a free shear layer in the supersonic regime. Only Peroomian and Kelly (1994) have studied the convective–absolute transition in a compressible supersonic flow, but in confined shear layers with constant mean temperature, density and pressure and for two-dimensional waves. They found that in the subsonic case, $M_1 < 1$, only one α_+ mode exists, and calculation of the transition boundary is straightforward. However, in the supersonic case multiple modes exist, and extreme care must be taken in the evaluation of the saddle point. This is due to the fact that when multiple modes exist in a system, coalescence can occur between two α_+ modes as well as α_+ and α_- modes. For $1 < M_1 < 1.32$, initially the subsonic/subsonic mode becomes absolutely unstable. However, if the backflow parameter is sufficiently increased, the subsonic/supersonic modes becomes the primary pinched mode, i.e., pinching for this mode occurs at a lower positive value of ω_{0_i}. At $M_1 = 1.32$, this change occurs at $\omega_{0_i} = 0$ and for $1.32 < M_1 < 1.35$ this change in the pinching of the modes occurs for a negative value of ω_{0_i}. For Mach numbers greater than 1.35, the primary mode is the subsonic/supersonic mode, and remains so up to the point near $M_1 \simeq 1.9$, where the mode becomes a supersonic/supersonic mode. Nevertheless, in their analysis, the three-dimensional and the temperature effects have not been taken into acount in the convective–absolute transition.

In this paper we examine the inviscid convective–absolute transition of a two- and three dimensional compressible free and confined shear layer with particular attention to the wall effect on this convective–absolute transition. In Section 2 we give general assumptions, the mathematical form of the perturbation and the mean flow. In Section 3 we formulate the stability problem and the boundary conditions and some general theoretical results are recalled. In Section 4 the numerical method used is briefly presented. Section 5 contains a presentation of our numerical results, in particular, the convective–absolute transition from a supersonic confined or not confined, isothermal or not isothermal, shear layer disturbed by oblique fluctuations is analyzed. To our knowledge, these cases were not studied in the literature. Conclusions are given in Section 6.

2. General Assumptions, Mathematical Form of the Perturbation and Mean Flow

The general equations of motion for the instantaneous flow are the Euler equations, the energy equation, written for the total energy, and the equation of state for a perfect gas. The boundary condition imposed in the present problem expresses that there is no variation of fluctuations far from the shear layer and that viscosity is not considered on the walls $\pm y_w$ (where y_w is the wall distance).

The present stability theory is based on the classical small perturbations technique where the instantaneous flow is the superposition of the known mean flow and unknown fluctuations. All the physical quantities q (velocity, pressure, ...) are decomposed into a mean value and a fluctuating one:

$$q(x, y, z, t) = \bar{q}(y) + q_f(x, y, z, t)\,, \tag{1}$$

where the mean flow is supposed to be parallel, i.e., it only depends on the y direction.

We consider a two-dimensional compressible shear layer, with zero pressure gradient, which separates two streams of different speeds and temperatures. We assume that the mean flow is governed by the compressible boundary layer equations. The x-axis is taken along the direction of the flow, the y-axis normal to the flow. Let $\overline{U}$, $\overline{V}$, 0 be the velocity components in the x^-, y^-, z-directions, respectively, let $\overline{\rho}$ be the density and let $\overline{T}$ be the temperature of this mean flow. All variables are nondimensionalized using upstream values at $y \to \infty$ or $y = +y_w$.

The structure of the mean flow clearly depends on the variation of the viscosity coefficient $\overline{\mu}$ and the Prandtl number P_r with the temperature and pressure. In general, both $\overline{\mu}$ and P_r are very weakly dependent on pressure and can be taken to be independent of pressure. The Prandtl number is somewhat dependent on the temperature but in this study it will be assumed to be constant. Finally, the dependence of viscosity on temperature is quite important and can be related to different thermodynamic models, see Jackson and

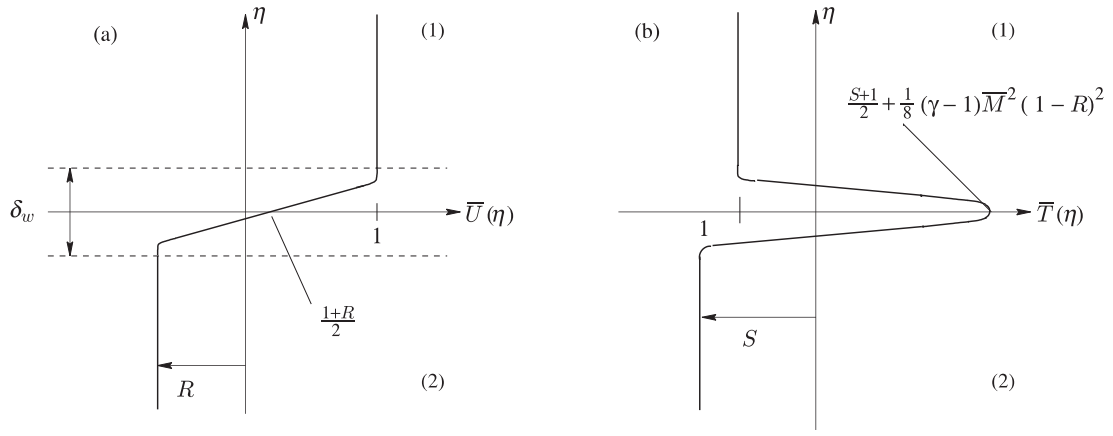

Figure 1. Sketch of different characteristics of the mean flow: (a) velocity profile, (b) temperature profile.

Grosch (1991a). However, as indicated in the Introduction, the various thermodynamic models give qualitatively similar results for a spatial stability analysis. As pressure is constant and the state equation is written in canonical for $\overline{\rho}\overline{T} = 1$. When the viscosity is supposed to be proportional to the temperature, that is we use the Chapman viscosity law, $\overline{\mu}(\overline{T}) = C\overline{T}$ and that $P_r = 1$, the solution of the mean flow equations has a similarity solution given by Lock (1951). However, as discussed in Jackson and Grosch (1991a), the qualitative stability characteristics are independent of the detailed shape of the mean profile. For this reason we use the Crocco relation, with the boundary conditions

$$\overline{U} \to 1, \quad \overline{T} \to 1 \quad \text{as} \quad \eta \to +\eta_w, \qquad \overline{U} \to R, \quad \overline{T} \to S \quad \text{as} \quad \eta \to -\eta_w, \qquad \eta_w \to \infty$$
$$\text{for the free shear layer}. \tag{2}$$

The temperature and velocity profiles are thus written as

$$\overline{T}(\eta) = S\frac{1-\overline{U}}{1-R} + \frac{\overline{U}-R}{1-R} + \frac{1}{2}(\gamma-1)\overline{M}_1^2(\overline{U}-R)(1-\overline{U}) \tag{3}$$

and

$$\overline{U}(\eta) = \frac{1}{2}\left[1 + R + (1-R)\tanh(\eta)\right], \tag{4}$$

where $\overline{U}$ is a good approximation of the Lock profile, γ is the ratio of specific heats and $\overline{M}_1$ is the Mach number defined as the ratio of the speed of the upper stream to the speed of sound. R and S are respectively the ratio of streamwise velocity and of temperature between the lower flow and the upper flow. The parameter range of interest for the velocity ratio is $-1 < R < 1$ and $S > 0$ for the temperature ratio. When $-1 < R < 0$, the low-speed stream is opposed to the high-speed stream and when $R > 0$ the two streams are coflowing. If S is less than 1, the lower stream is colder than the upper stream and if S is greater than Figure 1, the lower flow is warmer. Figure 1 shows the corresponding velocity and temperature profiles. The shear layer thickness is defined as $\delta_w = (1-R)/\max(\mathrm{d}\overline{U}/\mathrm{d}\eta)$. In this case, δ_w is equal to 2.

3. Stability Problem and General Theoretical Results

3.1. Linearized Euler Equations

The basic flow is perturbed by introducing wave disturbances for the velocity, pressure, temperature and density with amplitudes which are functions of y only. According to the homogeneous form of the boundary conditions, as well as the y-dependence of the mean flow (parallel assumption), the perturbation can

be described as a normal mode with respect to the x, z, t variables. Any perturbation (pressure, velocity, temperature, ...) can be written in the normal mode form

$$\mathbf{Z}_f(x, \eta, z, t) = \tilde{\mathbf{Z}}(\eta)\, \mathrm{e}^{i(\alpha x + \beta z - \omega t)}\,, \tag{5}$$

where $\tilde{\mathbf{Z}} = \left(\tilde{p}, \tilde{u}, \tilde{v}, \tilde{w}, \tilde{T}\right)^t$ is the function amplitude vector of the fluctuation, $\boldsymbol{k} = (\alpha, \beta)^t$ is a wave-number vector, with α and β the wave-numbers in the downstream (x) and cross-stream (z) directions, respectively, and ω is the circular frequency. In the general stability context, β is real, ω and α are *a priori* complex and their real parts are the magnitude of the frequency and the wave number, respectively, while their imaginary parts indicate whether the disturbance is amplified, neutral or damped depending on whether ω_i and $-\alpha_\mathrm{i}$ are negative, zero or positive. The decomposition (1) with the perturbation form (5) is introduced into instantaneous governing equations. The resulting equations are then simplified by taking into account, firstly, that the mean quantities satisfy the equations and, secondly, that the fluctuating quantities are assumed to be small, so that the equations can be linearized with respect to the disturbance. Finally, the linearized Euler equations lead to the well-known compressible Rayleigh equation written for the pressure. It is convenient to transform this equation into a form analogous to that for two-dimensional perturbations. Furthermore, we define $\hat{\alpha}^2 = \alpha^2 + \beta^2$ so that $\alpha = \hat{\alpha}\cos(\theta)$ and $\beta = \hat{\alpha}\sin(\theta)$, with θ the angle of propagation of the disturbance wave with respect to the flow direction ($\theta \in [0, \pi/2]$). Furthermore, we define $\hat{M}$ by $\hat{\alpha}\hat{M} = \alpha\overline{M}$. Applying this transformation to the compressible Rayleigh equation yields

$$\left\{ \frac{\mathrm{d}^2}{\mathrm{d}\eta^2} - \frac{2}{\overline{U} - c}\frac{\mathrm{d}\overline{U}}{\mathrm{d}\eta}\frac{\mathrm{d}}{\mathrm{d}\eta} - \hat{\alpha}^2\overline{T}\left[\overline{T} - \hat{M}^2\left(\overline{U} - c\right)^2\right] \right\} \tilde{p}(\eta) = 0\,. \tag{6}$$

Here c is the complex phase wave velocity $c = \omega/\alpha$. Equation (6) is solved with the following boundary conditions:

$$\lim_{\eta \to \pm\eta_\mathrm{w}} \frac{\mathrm{d}\tilde{p}}{\mathrm{d}\eta} = 0, \qquad \eta_\mathrm{w} \to \infty \quad \text{for free shear layer}\,. \tag{7}$$

For a given control parameter (R, S) and cross-stream wave-number β, (6) with the boundary condition (7) forms a linear eigenvalue problem for the parallel shear flow since a nonzero solution $\tilde{p}$ exists if and only if the complex set (α , ω) fulfills a relation $\mathcal{D}(\alpha, \omega; \beta, R, S) = 0$.

The purpose here is to define the propagative character of the unstable disturbances, i.e., to know if the basic flow is absolutely or convectively unstable, it is thus necessary to solve (6) and (7) along with the condition of zero group velocity

$$\mathcal{D}(\alpha_0, \omega_0; \beta, R, S) = 0 \quad \text{and} \quad \frac{\partial\mathcal{D}}{\partial\alpha}(\alpha_0, \omega_0; \beta, R, S) = 0 \tag{8}$$

and, in particular, the identification of these values (α_0, ω_0) corresponding to zeros of $\partial\omega/\partial\alpha$. The value ω_0 is, therefore, a square-root branch point of the function $\alpha(\omega)$ and the point α_0 in the complex α-plane corresponds to a saddle point formed by the intersection of upstream spatial branch $\alpha_+(\omega)$ and downstream spatial branch $\alpha_-(\omega)$. The nature of the instability is determined by the location of the branch point in the complex ω-plane. The instability is of absolute type if the branch point is in the upper half-plane ($\omega_\mathrm{i} > 0$) and is of convective type if it is in lower half-plane ($\omega_\mathrm{i} < 0$). Hence, the transition occurs for parameters values (i.e., R, S, $\overline{M}$) for which the branch point lies on the real ω-axis. This is essentially the Briggs–Bers criterion, see also Huerre and Monkewitz (1985).

3.2. Physical Nature of the Instability Modes

In order to know the physical nature of the mode solutions of our stability problem for the free shear layer, it is interesting to study the solution of (6) when the basic flow becomes independent of η, i.e., constant, typically when $\eta \to \infty$. When $\eta \to \infty$, (6) becomes

$$\left\{ \frac{\mathrm{d}^2}{\mathrm{d}\eta^2} - \hat{\alpha}^2\overline{T}\left[\overline{T} - \hat{M}^2\left(\overline{U} - c\right)^2\right] \right\} \tilde{p}(\eta) = 0\,, \tag{9}$$

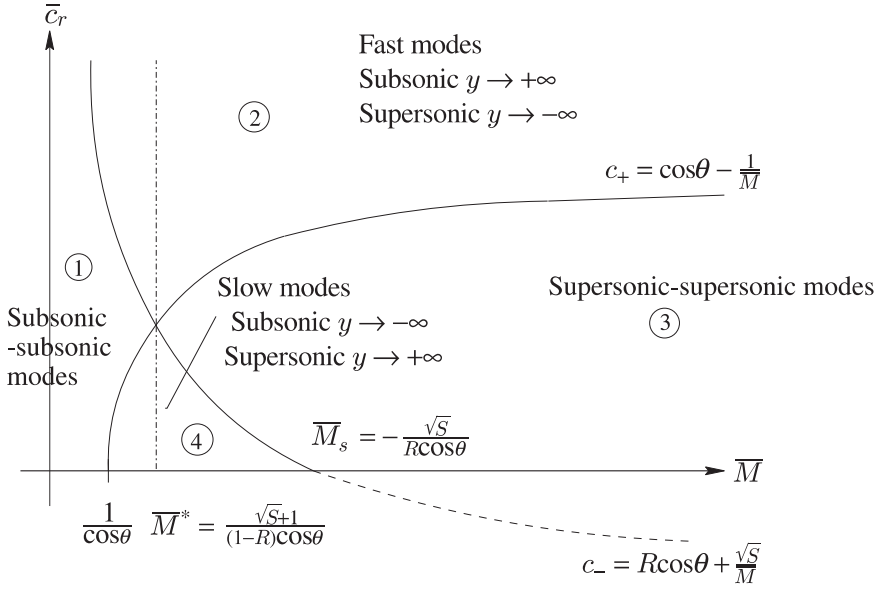

Figure 2. Classification of the modes in the Mach-number–phase-speed ($\overline{M}$, $c_\pm$) plane.

with $\overline{T}$ and $\overline{U}$ verifing the boundary conditions (2). The boundary conditions for $\tilde{p}$ are obtained by considering the limiting form of (6) as $\eta \to \pm\infty$. The solutions of (9) are of the form

$$\lim_{\eta\to+\infty} \tilde{p}(\eta) \propto \mathrm{e}^{-\Omega_+\eta} \quad \text{if} \quad c > c_+ \qquad \text{and} \qquad \lim_{\eta\to+\infty} \tilde{p}(\eta) \propto \mathrm{e}^{-i\eta\sqrt{-\Omega_+^2}} \quad \text{if} \quad c < c_+, \\ \text{with} \quad \Omega_+^2 = \hat{\alpha}^2\left[1 - \hat{M}^2\,(1-c)^2\right], \tag{10a}$$

$$\lim_{\eta\to-\infty} \tilde{p}(\eta) \propto \mathrm{e}^{+\Omega_-\eta} \quad \text{if} \quad c < c_- \qquad \text{and} \qquad \lim_{\eta\to+\infty} \tilde{p}(\eta) \propto \mathrm{e}^{-i\eta\sqrt{-\Omega_-^2}} \quad \text{if} \quad c > c_-, \\ \text{with} \quad \Omega_-^2 = \hat{\alpha} S\left[S - \hat{M}^2\,(R-c)^2\right]. \tag{10b}$$

We define $c_\pm$ as the phase speed for which $\Omega_\pm^2$ vanishes. Thus,

$$c_+ = 1 - \frac{1}{\hat{M}}, \qquad c_- = R + \frac{\sqrt{S}}{\hat{M}}. \tag{11}$$

Note that c_+ is the phase speed of a sonic disturbance in the high-speed side flow and c_- is the phase speed of a sonic disturbance in the low-speed side flow. At $\hat{M} = \hat{M}^* = (1+\sqrt{S})/(1-R)$, $c_\pm$ are equal. The nature of the disturbance and the appropriate boundary conditions can now be illustrated by Figure 2, where we plot $c_\pm$ versus $\overline{M}$ for typical values of R and S. This figure is a synthesis of different works of Jackson and Grosch (1989, 1990a, 1991a,b). These curves divide the (c_r, $\overline{M}$)-plane into four regions where c_r is the real part of c. If a disturbance exists with $\overline{M}$ and c_r in region 1 , then Ω_+^2 and Ω_-^2 are both positive, and the disturbance is subsonic at both boundaries. In region 3, Ω_+^2 and Ω_-^2 are both negative and hence the disturbance is supersonic at both boundaries. In region 2, Ω_+^2 is positive and Ω_-^2 is negative, and the disturbance is subsonic at $+\infty$ and supersonic at $-\infty$. Finally, in region 4, Ω_+^2 is negative and Ω_-^2 is positive so the disturbance is supersonic at $+\infty$ and subsonic at $-\infty$. This classification in the context of the convective–absolute transition gives a determination of the physical nature of the obtained modes. If the perturbation wave is subsonic at both $\pm\infty$ (region 1), one can choose the appropriate sign for $\Omega_\pm$ and have decaying solutions. We therefore have an eigenvalue problem. If the perturbation wave is supersonic at either or both boundaries, then the asymptotic solutions are purely oscillatory. These solutions are

of two types. It is clear that the oscillatory solutions are either incoming or outgoing waves. If one assumes that only outgoing waves are permitted, the problem of finding solutions in regions 2, 3 or 4 is again an eigenvalue problem wherein one chooses, as the boundary condition, the solution to (6) which yields outgoing waves in the far field. These characteristics have a fundamental importance in the confined shear layer case.

4. Numerical Resolutions

As clearly highlighted by Malik *et al.* (1985) and Malik (1990), the spectral collocation method based on Chebyshev polynomials provides an accurate and powerful tool when numerically solving the eigenvalue problem. The implementation of a spectral algorithm based upon collocation is almost as straightforward as the finite-difference scheme once the derivative matrices are set up. The use of collocation also simplifies the treatment of boundary conditions and coordinate transformations. In recent years, multidomain spectral methods have become fashionable for fluid mechanics problems. The method is described here for two domains. The physical domain $-\eta_w \le \eta \le \eta_w$ is divided into two domains $-\eta_w \le \eta \le \eta_i$ and $\eta_i \le \eta \le \eta_w$ which may be denoted as domain I and domain II, respectively. In this paper η_i is the altitude of the generalized inflection point $\mathrm{d}(\overline{T}^{-2}\mathrm{d}\overline{U}/\mathrm{d}\eta)/\mathrm{d}\eta|_{\eta_i} = 0$. Note that this expression differs from that given by Lee and Lin (1946) by a factor $\overline{T}^{-1}$ because they wrote this expression in terms of y and we have chosen, like Jackson and Grosch (1989), to write it in terms of η. The stability equation (6) now may be written in the two domains as

$$D_I^2\tilde{p}_I + A_I D_I \tilde{p}_I + B_I \tilde{p}_I = 0 \quad \text{and} \quad D_{II}^2\tilde{p}_{II} + A_{II} D_{II}\tilde{p}_{II} + B_{II}\tilde{p}_{II} = 0, \qquad \text{with} \qquad D_I = D_{II} \equiv \frac{\mathrm{d}}{\mathrm{d}\eta},$$

and with the boundary conditions $D_I\tilde{p}_I = 0$ as $\eta \to -\eta_w$ and $D_{II}\tilde{p}_{II} = 0$ as $\eta \to +\eta_w$. In addition, we need interface conditions at $\eta = \eta_i$. These are provided by requiring the derivability of $\tilde{p}$ at $\eta = \eta_i$, i.e., $D_I\tilde{p}_I(\eta_i) = D_{II}\tilde{p}_{II}(\eta_i)$. The physical domains $-\eta_w \le \eta \le \eta_i$ and $\eta_i \le \eta \le +\eta_w$ are now transformed to the computational domains. We use Nth-order Chebyshev polynomials T_N defined in the interval $-1 \le \xi_j^i \le 1$, $i = \mathrm{I}\,\mathrm{or}\,\mathrm{II}$, where the collocation points ξ_j^i are the extrema of T_n and are given by

$$\xi_j^i = \cos\frac{\pi j}{N_i}, \qquad j = 0, \ldots, N_i, \quad i = \mathrm{I}\,\mathrm{or}\,\mathrm{II}. \tag{12}$$

The Chebyshev collocation method is applied separately to the two domains with collocation points. In order to apply the spectral collocation method, an interpolant polynomial is constructed for the dependent variables in terms of their values at the collocation points. Thus an Nth-order polynomial may be written as

$$\tilde{p}_i(\xi^i) = \sum_{k=0}^{N_i} a_k^i(\xi^i)\,\tilde{p}_i(\xi_k), \qquad i = \mathrm{I}\,\mathrm{or}\,\mathrm{II}, \tag{13}$$

where the interpolant $a_k^i(\xi^i)$ for the Chebyshev scheme is given by

$$a_k^i(\xi^i) = \left(\frac{1-\xi_k^2}{\xi^i - \xi_k}\right)\frac{T_N'(\xi^i)}{N^2 c_k}(-1)^{k+1}, \qquad \text{where} \qquad c_0 = c_N = 2, \quad c_k = 1, \quad \text{for} \quad k \in \{1, \ldots, N-1\},$$

and $\quad i = \mathrm{I}\,\mathrm{or}\,\mathrm{II}$.

The first derivative of $\tilde{p}_i(\xi^i)$ may be written as

$$\left.\frac{\mathrm{d}\tilde{p}_i}{\mathrm{d}\xi^i}\right|_j = \sum_{k=0}^{N_i} E_{jk}^i\,\tilde{p}_{i,k}, \qquad i = \mathrm{I}\,\mathrm{or}\,\mathrm{II}, \tag{14}$$

where E^i_{jk} are the elements of the derivative matrix given by

$$E^i_{jk} = \frac{c_j}{c_k}\frac{(-1)^{k+j}}{\xi^i_j - \xi^i_k}, \quad j \neq k, \qquad E^i_{jj} = -\frac{\xi^i_j}{2\left(1-\xi^{i\,2}_j\right)}, \qquad E^i_{00} = \frac{2N_i^2+1}{6} = -E^i_{N_iN_i}, \qquad i = \mathrm{I\,or\,II}\,.$$

The scaling factor for the transformation between physical and computational domains is given as $S^i_j = \partial\xi^i/\partial\eta\,|_j$, $j = 0, \ldots, N_i$, then the first derivative matrix F in the physical domain may be written as

$$F^i_{jk} = S^i_j E^i_{jk}\,, \tag{15}$$

and the second derivative matrix G^i_{jk} is simply $G^i_{jk} = F^i_{jm}F^i_{mk}$. Now the stability equation (6) may be written at the collocation points ξ^i_j as

$$\sum_{k=0}^{N_i} G^i_{jk}\tilde{p}_{i,k} + A^i_j \sum_{k=0}^{N_i} F^i_{jk}\tilde{p}_{i,k} + B^i_j\tilde{p}_{i,k} = 0, \qquad i = \mathrm{I\,or\,II}\,. \tag{16}$$

Finally, (16) with the boundary conditions $D_i\tilde{p}_i(\pm y_\mathrm{w}) = 0$ may be represented as

$$\left(\underline{\underline{C_3}}\alpha^3 + \underline{\underline{C_2}}\alpha^2 + \underline{\underline{C_1}}\alpha + \underline{\underline{C_0}}\right)\underline{\boldsymbol{\phi}} = 0, \qquad \text{with} \quad \underline{\boldsymbol{\phi}} = (\tilde{p}_0, \ldots, \tilde{p}_N)^t \quad \text{where} \quad N = N_1 + N_2. \tag{17}$$

Equation (17) represents the discretized eigenvalue problem. The Chebyshev interval $-1 \le \xi \le 1$ is transformed to the computational domain $-\eta_\mathrm{w} \le \eta \le \eta_\mathrm{w}$ by use of the mapping

$$\eta_\mathrm{I} = -\frac{\eta_\mathrm{w}}{2}(\xi_\mathrm{I}+1)\,, \qquad \eta_\mathrm{II} = \frac{\eta_\mathrm{w}}{2}(1-\xi_\mathrm{II})$$

for the confined shear layer and for the free shear layer ($\eta_\mathrm{w} \to \infty$) the mapping

$$\eta_\mathrm{(I,II)} = a\frac{\xi_\mathrm{(I,II)}+1}{b-\xi_\mathrm{(I,II)}}, \qquad \text{with} \quad a = \frac{\eta_\mathrm{a}\eta_\mathrm{w}}{(\eta_\mathrm{w}-2\eta_\mathrm{a})} \quad \text{and} \quad b = 1+\frac{2a}{\eta_\mathrm{w}}\,,$$

is used. In our case $\eta_\mathrm{a} \simeq \delta_\mathrm{w}$, where δ_w is the shear layer thickness. A standard eigenvalue subroutine may now be used to compute the $N+1$ eigenvalues. Two methods were used to solve (17): a local method based on a shooting method with a classical Newton–Raphson algorithm and a global method, where the discretized operator spectrum is computed, see Bridges and Morris (1984). In the results presented below, the number of points in each domain is respectively $N_1 = 100$ and $N_2 = 200$ for the free shear layer and $N_1 = 100$ and $N_2 = 100$ for the confined shear layer.

To determine the convective–absolute transition, the saddle point for the present system is found by three different numerical techniques. The first method involves the calculation of the branches $\alpha^+(\omega)$ and $\alpha^-(\omega)$ corresponding to $x > 0$ and $x < 0$, respectively, for different ω until pinching is observed. The second is a Taylor series fit near the saddle point, which is a square-root branch point in the complex wave-number plane. The third is a direct numerical method using Newton–Raphson's technique for solving $\partial\omega/\partial\alpha = 0$. However, this last method is highly dependent on the initial guess provided for the saddle point location, and once the solution converges, it cannot be said without *a priori* knowledge whether the converged solution is the location of a coalescence of two α^+ modes or of an α^+ mode and an α^- mode. In this study the first method is systematically used with the second method. Occasionally, the third method is employed as a check of our results.

5. Results

In this section the case of convective–absolute transition in free and confined shear layers is studied. Results are presented, and in particular the amount of backflow necessary to have this type of transition for a range of primary flow Mach numbers $\overline{M}_1$ up to 3.0. The boundary of the convective–absolute (CA) transition is defined as a function of the velocitity ratio R, the temperature ratio S, the Mach number $\overline{M}_1$ and the angle of the obliquity of the disturbance θ with respect to the flow direction.

5.1. Free Shear Layer

5.1.1. Two-Dimensional Instability Wave and Isothermal Flow

Three sets of results have been obtained, which are presented here. First, the variation of the velocity ratio and stability parameters with Mach number $\overline{M}_1$ under the requirement that the square-root branch point of $\alpha(\omega)$ lies on the real ω-axis (CA transition) for isothermal ($S = 1$) flow is shown. Second and third, the variation of these same parameters with temperature ratio S or the angle of the propagation of the disturbance wave θ, respectively, for a prescribed Mach number $\overline{M}_1$, requiring again that the branch point is located on the real ω-axis, is also shown. The pertinent stability parameters in each case are the real branch point frequency ω_{0_r} and the real and the imaginary parts of the wave number (α_{0_r}, α_{0_i}) of the corresponding saddle point in the α-plane. Figure 3 gives the parametric variation of the critical branch point location separating the domains of absolute and convective instabilities in the (R, $\overline{M}_1$)-plane for the isothermal shear layer. The intercept value of R at $\overline{M}_1 = 0$ coincides with the value -0.136 computed by Huerre and Monkewitz (1985). Figure 3(a) shows that the shear flow remains convectively unstable with increasing backflow on the low-speed side as the Mach number increases. This trend remains true for $\overline{M}_1 \leq 1.448$. In fact, for this Mach number range, the phase speed of the instability wave is subsonic (zone 1 in Figure 2). Our results differ from those of Pavithran and Redekopp (1989) by at most 10% because their temperature profile is not given by the Crocco relation. Instead, their temperature equation is equivalent to that obtained from (3) by dropping the Mach squared term. Jackson and Grosch (1990b) have obtained similar results, who, unlike Pavithran and Redekopp (1989), did not neglect the Mach number square term in the temperature profile. However, in their analysis, the CA transition is limited to the subsonic isother-

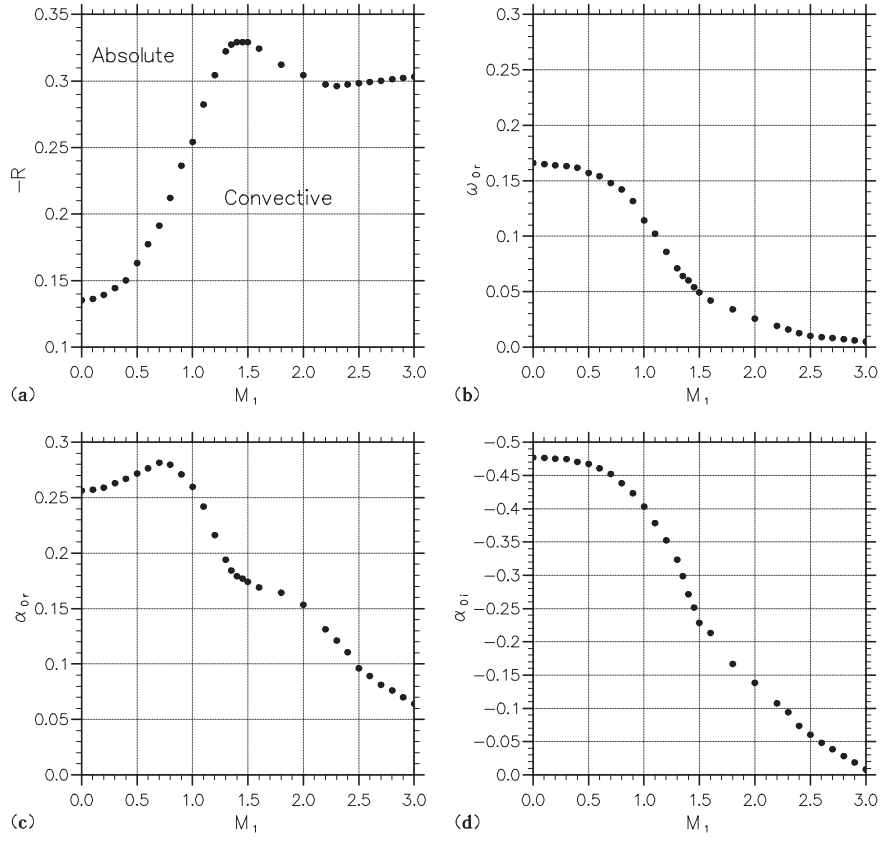

Figure 3. The CA transition boundary (a) and variation of the branch point parameters with high-speed side Mach number $\overline{M}_1$: (b) circular frequency ω_0; (c) wave-number α_{0_r}; (d) the spatial growth rate α_{0_i} for two-dimensional disturbance ($\theta = 0°$) and isothermal shear layer ($S = 1$).

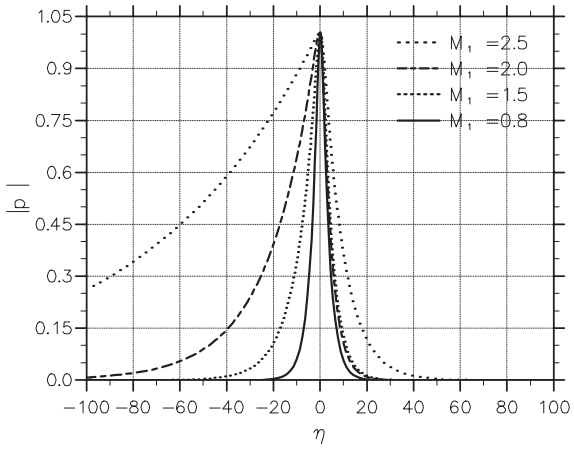

Figure 4. Eigenfunctions (pressure amplitude) for different Mach numbers, $\overline{M}_1 = 0.8$, 1.5, 2.0 2.5, for $S = 1$, $\theta = 0°$ and with $\pm\eta_w = 300$.

mal shear layer with a two-dimensional disturbance ($\theta = 0°$). Our results are within 2% of their results. To our knowledge, study of the CA transition for a supersonic shear layer was not carried out. When the Mach number is greater than 1.448, the phase speed of the instability wave becomes supersonic at $+\infty$ and subsonic at $-\infty$ (zone 4 in Figure 2), the evolution of the CA transition boundary changes in this regime. When the phase speed of the instability wave becomes supersonic, the boundary of the CA transition continues to increase until $\overline{M}_1 \simeq 1.5$ ($-R \simeq 0.33$) and it stabilizes around $R = -0.3$ when $\overline{M}_1 > 2.1$. The variation of the branch point parameters with the Mach number is given in Figure 3b–d. The trends are monotonic with the Mach number, except for the real part of the wave number. The decrease of α_{0_i}, as $\overline{M}_1$ tends to unity, may be associated with the stabilization of the continuation of the Kelvin–Helmholtz instability in incompressible flow and the decreasing bandwidth of unstable wave numbers α_r for this mode. The branch point frequency decreases substantially for Mach numbers above 0.3, where compressibility effects become significant. For these branch point parameters, the modification of the instability wave nature can be seen from a slope change in their evolutions with respect to Mach number. When the Mach number increases, the absolute frequency ω_0 (Figure 3(b) and the absolute spatial growth rate α_{0_i} (Figure 3(d)) tend towards zero. For a high Mach number ($\overline{M}_1 \geq 3$) the CA transition loses its significance because the absolute spatial growth rate is close to zero. However, it should be remembered that additional modes of instabiliy are present for $\overline{M}_1$ greater than unity. Indeed, the works of Jackson and Grosch (1989) and Mack (1989) have shown, for a purely spatial instability, that there are supersonic modes. However, for $\bar{M}_1 \leq 3$ these modes are not dominant in the CA transition for a free shear layer (no pinching has been observed). Figure 4 shows typical pressure eigenfunction instability waves for several Mach numbers. As the Mach number increases, the decrease of the pressure fluctuation on the low-speed side is increasingly weak. This characteristics is representative of the supersonic phase speed of the instability wave.

5.1.2. Three-Dimensional Instability Wave and Isothermal Flow

For a three-dimensional instability wave, when the Mach number is less than 1, the amount of backflow necessary for transition from convective to absolute instability increases with the angle of the disturbance. When $\overline{M}_1 > 1$, the opposite trend is found. A three-dimensional wave is more favorable to the CA transition. Figure 5(a) shows this evolution for three Mach numbers. For $\overline{M}_1 = 0.8$, the phase speed of the instability wave is always subsonic for any angle θ. For $\overline{M}_1 = 1.5$ and for $\overline{M}_1 = 2.0$, the instability wave is always supersonic, when $\theta < 20.8°$ (for $\overline{M}_1 = 1.5$) and $\theta < 43.1°$ (for $\overline{M}_1 = 2.0$); the speed wave is in zone 4, otherwise the speed wave is in zone 3. The variation of the branch point parameters with the angle of the perturbation θ is monotonic, the evolution of these parameters depends on the Mach number $\overline{M}_1$. If $\overline{M}_1 < 1$, then ω_0 and α_{0_r} decrease and α_{0_i} increases; and if $\overline{M}_1 > 1$ the opposite trends are found.

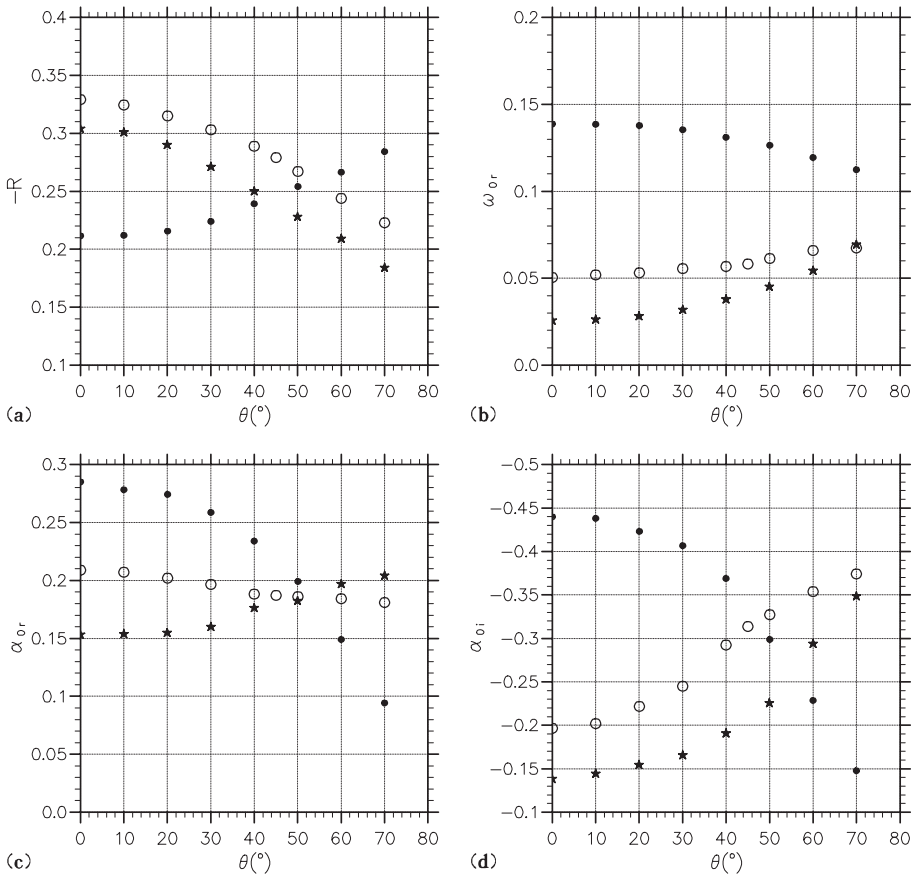

Figure 5. The CA transition boundary (a) and variation of the branch point parameters versus θ: (b) circular frequency ω_0; (c) wavenumber α_{0_r}; (d) the spatial growth rate α_{0_i} for different Mach numbers, $\overline{M}_1 = 0.8$ (•), 1.5 (○), 2.0 (⋆), and for an isothermal shear layer ($S = 1$).

5.1.3. Two-Dimensional Instability Wave and Nonisothermal Flow

The influence of the temperature ratio S on the CA transition boundary is shown in Figure 6. It is clear that the temperature ratio has a larger influence than the Mach number on the transition velocity ratio over the entire range. It is observed that cooling the low-speed side can causes a convectively unstable shear layer at a fixed velocity ratio to become absolutely unstable. When $S < 1$, only a small amount of backflow is required on the low-speed side ($\overline{U}_2 = -0.0745\overline{U}_1$, for a subsonic compressible flow ($\overline{M}_1 = 0.8$)). These results are consistent with the calculations presented by Pavithran and Redekopp (1989). The transition velocity ratio for $\overline{M}_1 = 0.8$ was calculated for $S = 0.1$ and $S = 10$, we have obtained $R = -0.0745$ and $R = -0.745$, respectively. These values are within about 1% of those reported by Pavithran and Redekopp (1989) ($R = -0.074$ and $R = -0.74$, when they used the temperature profile obtained by Crocco's relation). The variation of the branch point parameters with the temperature ratio for a subsonic Mach number ($\overline{M}_1 = 0$ and 0.8) are close to those obtained by Pavithran and Redekopp (1989) and Jackson and Grosch (1989). These evolutions are presented in Figure 6(b)–(d). In a supersonic regime the evolution of the branch point parameters can be qualitatively different. When the temperature ratio changes, the nature of the instability also changes. For example, if $\overline{M}_1 = 2$ and if $S < 0.4$, then the phase speed of the instability wave is supersonic/supersonic (in zone 3). On the other hand, if $0.4 \leq S \leq 3.225$ the phase speed is subsonic/supersonic but pertaining to zone 4. Finally, if $S > 3.225$ the phase speed is always subsonic/supersonic (in zone 4) but with $\overline{M}_1 < \overline{M}^*$. In this last case, the evolution of the absolute wave number (α_{0_r} and α_{0_i}) is qualitatively different (see Figure 6(c)–(d)).

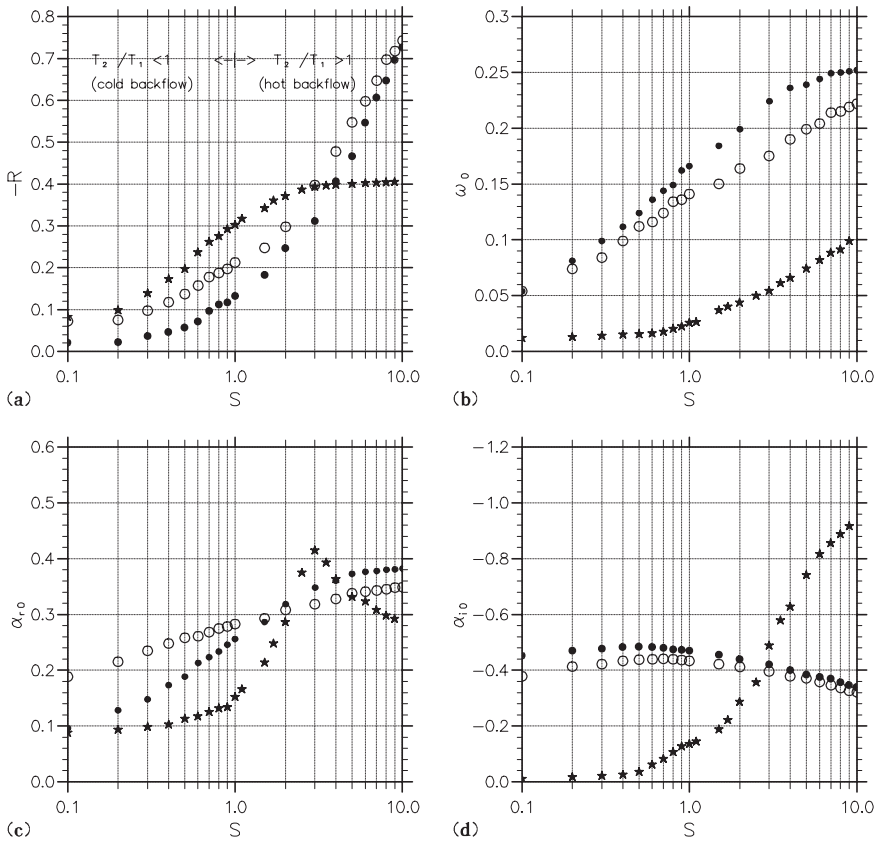

Figure 6. The CA transition boundary (a) and variation of the branch point parameters versus $S = \overline{T}_2/\overline{T}_1$: (b) circular frequency ω_0; (c) wave-number α_{0_r}; (d) the spatial growth rate α_{0_i} for different Mach numbers, $\overline{M}_1 = 0$ (•), 0.8 (○), 2.0 (⋆), and for a two-dimensional perturbation ($\theta = 0°$).

5.2. Confined Shear Layer

5.2.1. Two-Dimensional Instability Wave and Isothermal Flow

In this section the local two- and three-dimensional stability characteristics of a confined compressible shear layer are studied. The mean flow is defined as in the previous section, the mean velocity profile is modeled as a finite length shear layer with a hyperbolic tangent velocity profile (4) and the mean temperature profile is given by Crocco's relation (3). The walls are localized, in a first step, at $\eta = \pm\eta_w$ with $\eta_w = 10$. At this distance, the mean flow is uniform. These boundary conditions are identical to those chosen by Peroomian and Kelly (1994). However, in their case the mean temperature, density and pressure have been chosen constant and the instability wave sought was two-dimensional.

Figure 7(a) shows the backflow necessary for transition between convective and absolute instability for different values of the Mach number $\overline{M}_1$. The subsonic portion of Figure 7(a) qualitatively agrees (about 2%) with the work of Pavithran and Redekopp (1989) and of Jackson and Grosch (1989). The amount of backflow necessary for transition from convective to absolute instability increases as the Mach number increases. In the subsonic case the wall effect does not influence the CA transition. However, the branch point parameters (ω_0, α_0) are affected. For a confined subsonic shear layer, the absolute frequency is close to that obtained for a free shear layer, but this is not the case for the absolute wave number. In the confined case the absolute wavelength is almost twice larger, and the absolute growth rate is 1.6 weaker than in the case of the free shear layer (see Figure 3). For the subsonic case, $\overline{M}_1 < 1.0$, only one α_+ mode exists, but in the supersonic case multiple modes exist, and extreme care must be taken in the evaluation of the saddle point. This is due to the fact that when multiple modes exist in the system, coalescence can occur between two α_+ branches as well as an α_+ and an α_- branch. In Figure 7(a), once the mean flow becomes supersonic, the

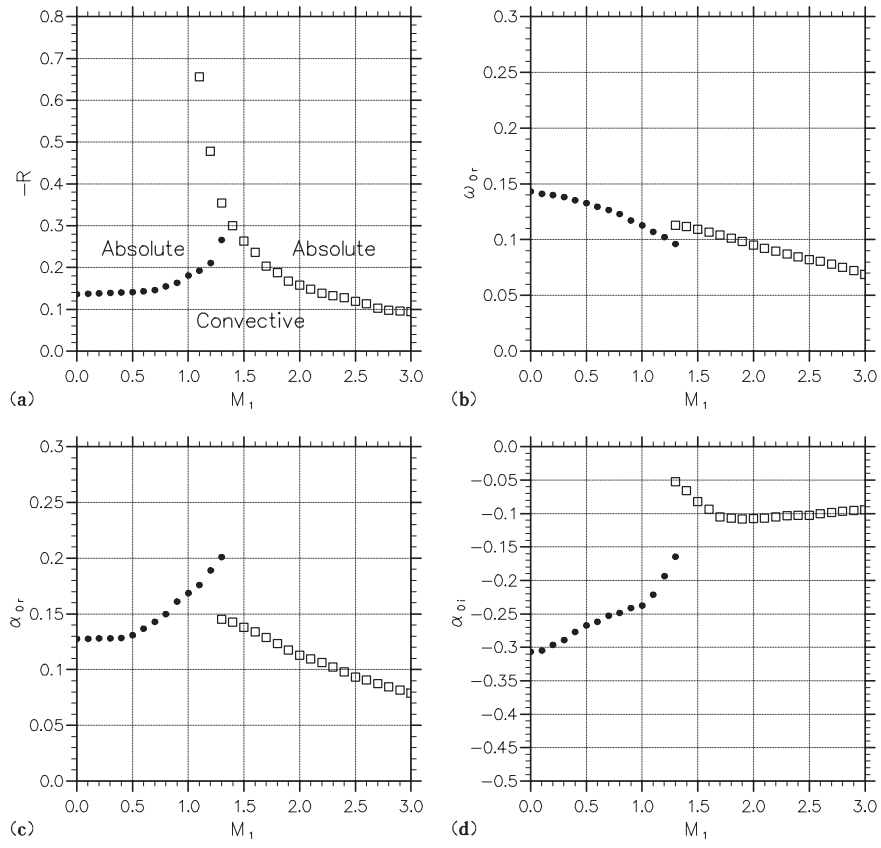

Figure 7. The CA transition boundary (a) and variation of the branch point parameters with upper-layer Mach number $\overline{M}_1$: (b) circular frequency ω_0; (c) wave-number α_{0_r}; (d) the spatial growth rate α_{0_i} for two-dimensional disturbance ($\theta = 0°$) and isothermal shear layer ($S = 1$). •, mode 1; □, mode 2.

characteristics of the transition boundary change. The absolutely unstable mode for the subsonic Mach numbers remains the dominant mode when $1.0 < \overline{M}_1 < 1.32$ (dominant in the sense that it becomes absolutely unstable for the smallest $-R$ value). The associated phase speed with this mode is subsonic/subsonic (called mode 1). However, another mode exists but it is not dominant for this Mach number range, this mode is subsonic/supersonic. Indeed, if one increases the backflow parameter sufficiently, the subsonic/supersonic mode (called mode 2) becomes the primary mode, i.e., pinching for this mode occurs at a lower positive value of ω_{0_i}. At $\overline{M}_1 = 1.32$, where the cusp in the curve is located (see Figure 7), this change occurs at $\omega_{0_i} = 0$. For $1.32 < \overline{M}_1 < 1.345$, this change in the pinching of the modes occurs for a negative ω_{0_i}. Figure 8 shows the evolution of the imaginary part of the absolute frequency ω_{0_i} for different Mach numbers. In the case $\overline{M}_1 = 1.25$, the first mode becomes absolutely unstable when $-R > 0.22$ and it becomes again unstable convectively when $-R > 0.47$. For this Mach number, the second mode becomes absolutely unstable for $-R > 0.42$. For $\overline{M}_1 = 1.32$, the transition from convective to absolute (CA), for mode 1, occurs when $-R = 0.26$ and the reverse transition, from absolute to convective (AC), occurs when $-R = 0.35$. For the second mode, the CA transition occurs when $-R = 0.356$. In fact, for $1.32 < \overline{M}_1 < 1.345$, a small region exists between $0.35 < -R < 0.356$ where the two modes are convectively unstable. This corresponds to the region in Figure 7(a), where the boundary has turned back on itself near the cusp. Beyond this Mach number, $\overline{M}_1 = 1.345$, mode 1 is not absolutely unstable, only mode 2 becomes absolutely unstable. Figure 8 shows this characteristic for $\overline{M}_1 = 1.4$. For Mach numbers greater than 1.345, the primary mode is the subsonic/supersonic mode, and remains so up to the point near $\overline{M}_1 \simeq 1.95$, where the mode becomes a supersonic/supersonic mode. This mode selection, which is dependent on R, was already observed by Peroomian and Kelly (1994), but they had not taken into account the mean temperature profile, which is clearly nonconstant for these Mach number ranges. However, our results are close to those obtained by Peroomian and Kelly (1994) (within between 1% and 5%). For the temperature profile given by Crocco's relation,

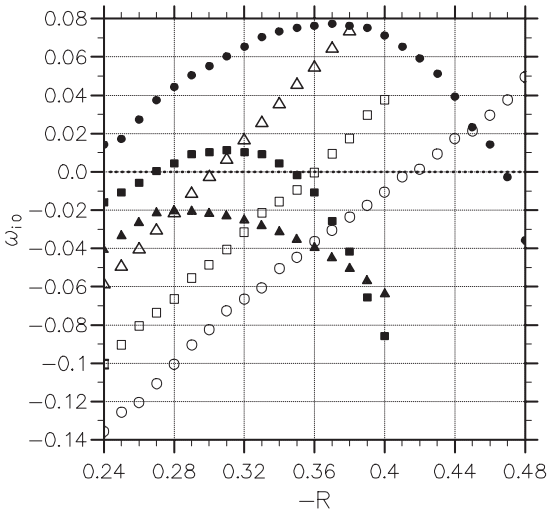

Figure 8. Imaginary part of saddle point frequency versus the backflow parameter R for different Mach numbers: $\overline{M}_1 = 1.25$, •, mode 1, ∘, mode 2; $\overline{M}_1 = 1.32$, ■, mode 1, □, mode 2; $\overline{M}_1 = 1.4$, ▲, mode 1, △, mode 2.

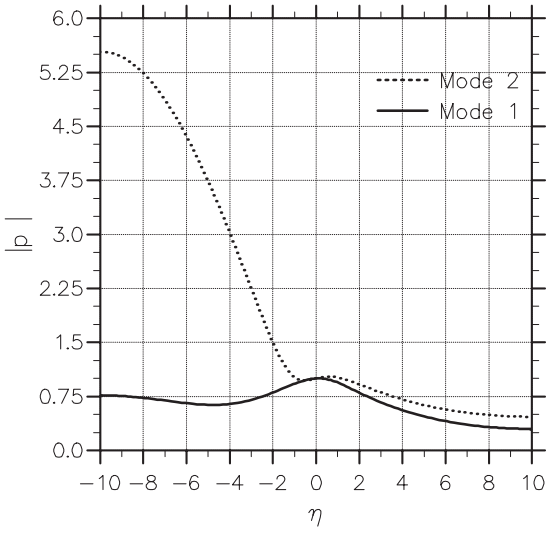

Figure 9. Eigenfunctions (pressure amplitude) for the modes 1 and 2, for $\overline{M}_1 = 1.31$, $S = 1$, $\theta = 0°$ and with $\pm\eta_w = 10$.

the CA transition occurs for a lower value of the backflow than in the case where the temperature profile is constant.

Physically, in the linear stability context, this shows that in the region between $1.32 < \overline{M}_1 < 1.345$, as the backflow parameter increased, the flow becomes absolutely unstable. If the backflow is further increased, the mode becomes convectively unstable once again, and a further increase in backflow will make a different mode absolutely unstable. This is due to the fact that multiple modes exist when $\overline{M}_1 > 1$. When the backflow parameter is increased for a fixed $\overline{M}_1$, the shear is increased and the spatial growth rate for the subsonic/subsonic mode decreases; the spatial growth rate for the subsonic/supersonic increases, this eventually causes the subsonic/supersonic mode to become the primary pinched mode. However, further increase in the backflow causes a jump in the branch point parameters. Indeed, this occurs for the same R, S, $\overline{M}_1$ and ω_{0_i} but for a different ω_{0_r}, α_{0_r} and α_{0_i}.

Table 1 shows the wall influence on the CA transition for mode 2. When $|\eta_w|$ increases, the backflow required to achieve the CA transition decreases but the absolute spatial growth rate also decreases until becoming neutral, at this distance, $|\eta_w| \simeq 24$, the CA transition does not exist. For a supersonic shear

Table 1. Wall effects on the CA transition for mode 2: $\overline{M}_1 = 1.32$, $S = 1$ and $\theta = 0$.

$\lvert\eta_w\rvert$	R	ω_0	α_0
07	−0.387	0.1660	0.208–0.093i
08	−0.380	0.1450	0.184–0.076i
09	−0.372	0.1288	0.168–0.064i
10	−0.356	0.1135	0.146–0.059i
11	−0.353	0.1043	0.135–0.044i
12	−0.350	0.0953	0.126–0.034i
14	−0.348	0.0807	0.108–0.023i
17	−0.346	0.0757	0.088–0.015i
20	−0.340	0.0551	0.072–0.0089i
>24, the CA transition does not exist.			

layer, the existence of a wall plays a determining role in the characterization of instabilities. Figure 9 shows typical eigenfunction (pressure) distributions of subsonic/supersonic instability waves (mode 2) and subsonic/subsonic instability waves (mode 1).

5.2.2. Three-Dimensional Instability Wave and Isothermal Flow

For a three-dimensional instability wave, when the Mach number is subsonic, the CA transition first occurs for a two-dimensional wave, this characteristic is identical to that obtained for the free subsonic shear flow, but the evolution of the branch point parameters are not the same. The main difference between the subsonic confined case and the subsonic free case lies in the spatial growth rate $-\alpha_{0_i}$. In the free shear flow, when $\overline{M}_1 < 1$, the evolution of $-\alpha_{0_i}$ is decreasing with increasing θ, while in the confined shear flow the spatial growth rate increases. This characteristic is thus directly related to the wall effect. These facts occur for all $\overline{M}_1 < 1$. Indeed, when the walls are moved away, the evolution of the absolute spatial growth rate versus θ tends to the solution obtained when there is no wall. Again in this case, when $|\eta_w| \simeq 20$, the wall effects on the CA transition are not decisive. When the mean flow is supersonic, multiple modes exist Tam and Hu (1989), Mack (1989). In the last section we have shown, in the case of a two-dimensional disturbance, for $\overline{M}_1 > 1.32$, that the CA transition was not realized by the pinching from subsonic/subsonic modes but by the pinching between two subsonic/supersonic modes. It is always the case for the three-dimensional instability wave, the two modes in CA transition, according to whether mode 1 or mode 2 is dominating, always exist. However, this change of mode depends on the angle θ and more exactly on the physical nature of the instability waves. The results presented in Figure 10(a) show that CA transition occurs initially for a two-dimensional wave. This result is in agreement with those presented by Tam and Hu (1989), for a purely spatial instability. According to Tam and Hu (1989), these spatial supersonic instability waves are generated by a Mach wave system formed by reflections from the channel walls. These modes only exist when the convective Mach numbers of the flow on both sides of the shear layer are supersonic. Figure 10 shows the evolution of the characteristics of the CA transition according to the disturbance angle θ for four different Mach numbers.

5.2.3. Two-Dimensional Instability Wave and Nonisothermal Flow

The influence of the temperature ratio (S) on the CA transition boundary is shown in Figure 11. Again in this case, it is clear that the temperature ratio has a large influence on CA transition. As for the free shear flow, it is observed that the cooling of the low-speed side can cause a convectively unstable shear layer at a fixed velocity ratio to become absolutely unstable. This effect seems to be true for a large Mach number range ($0 < \overline{M}_1 < 3.0$). However, there exists a significant difference in the influence of S on the CA transition for a free shear layer and for a confined shear layer. This can be found in the evolution of α_0 when the instability wave has, at least, its phase speed supersonic in one of the shear layer sides. Figures 6(c),(d) and 11(c),(d) show these differences.

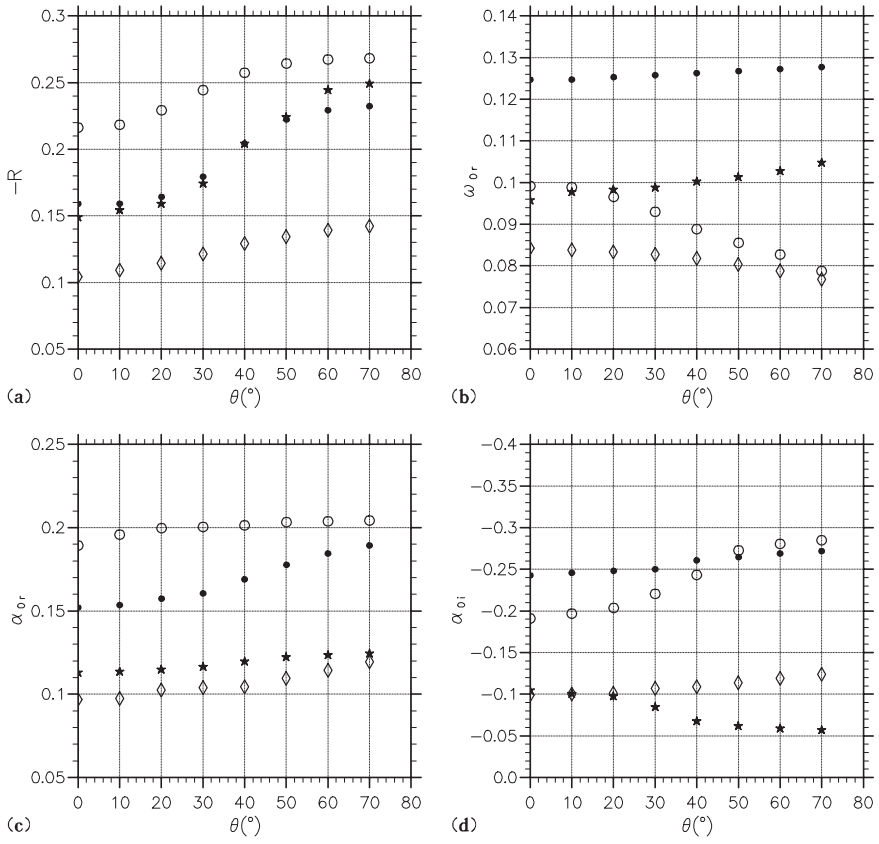

Figure 10. The CA transition boundary (a) and variation of the branch point parameters versus θ: (b) circular frequency ω_0; (c) wavenumber α_{0_r}; (d) the spatial growth rate α_{0_i} for different Mach numbers, $\overline{M}_1 = 0.8$ (•), 1.2 (○), 2.0 (⋆) 2.5 (◇), and for an isothermal shear layer ($S = 1$).

5.3. Some Wall Effects

Figure 12 shows the wall effects on the CA instability transition boundaries for an incompressible isothermal shear layer and for a two-dimensional instability wave. The instability is of absolute type whenever $-R$ exceeds the value along the curves shown in this figure. When the plane wall is placed on the low-speed side, there is an initial departure from the free shear layer transition value near $-\eta_w \simeq 15$. The curve soon rises to progressively higher values of $-R$ as the wall is moved closer to the shear layer. When the wall is placed on the high-speed side, there is an initial departure from the free shear layer transition value to the higher values of $-R$ around $+\eta_w \simeq 10$. However, when the wall is moved still closer to the shear layer ($+\eta_w \simeq 5$), the CA transition boundary strongly decreases. When the two walls move, the effect on the CA transition boundary is roughly an average effect of the influence of the two walls separately. This behavior is qualitatively identical for all subsonic Mach numbers ($\bar{M}_1 < 1$) and for all subsonic two-dimensional instability waves. In all cases, for an incompressible shear layer, the wall effect on the CA transition becomes important when the wall (lower and/or upper) is very close to the shear layer (the wall distance is close to the shear layer thickness). In fact, when the distance between the walls and the shear layer is close to the shear layer thickness, the strictly parallel assumption of flow is not checked, the nonparallel effects are not negligible and the results obtained with the parallel assumption are thus to be taken with caution.

In the supersonic regime the behavior is more complex due to the existence of multiple modes strongly influenced by the wall. This was explored by making computations which differ slightly from the incompressible case presented above: the high and low walls were placed symmetrically, and the calculations were performed for various distances between them. In this part we are interested in the link between CA transition observed in the free shear layer (Section 5.1) and CA transition observed in the confined shear layer

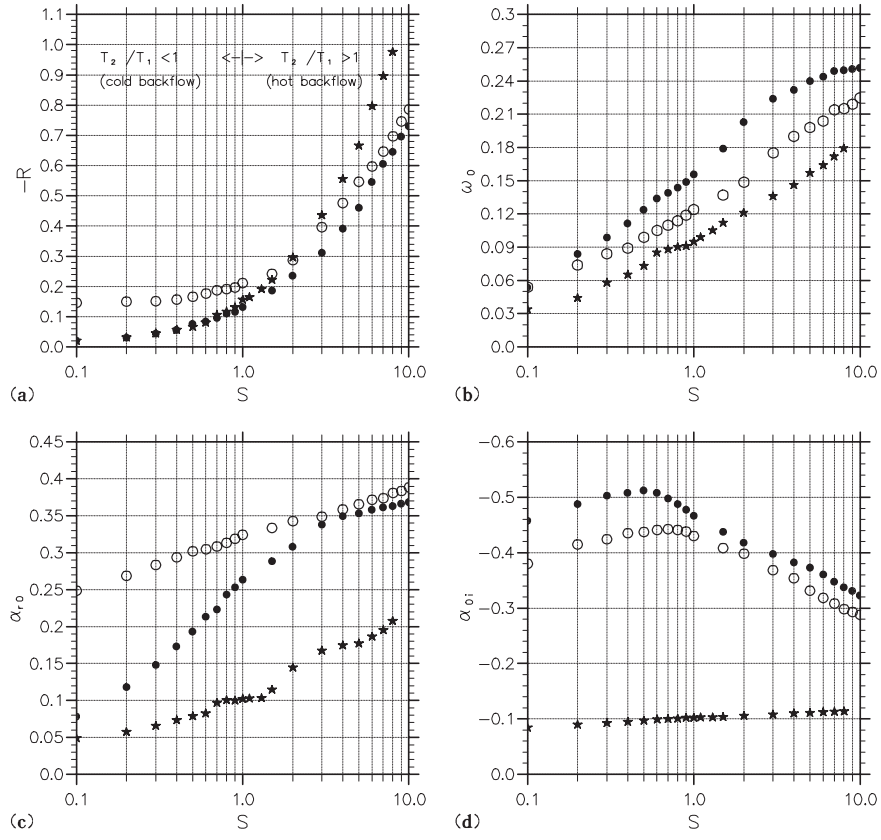

Figure 11. The CA transition boundary (a) and variation of the branch point parameters versus $S = \overline{T}_2/\overline{T}_1$: (b) circular frequency ω_0; (c) wave-number α_{0_r}; (d) the spatial growth rate α_{0_i} for different Mach numbers, $\overline{M}_1 = 0$ (•), 0.8 (○), 2.0 (⋆), and for two-dimensional perturbation ($\theta = 0°$).

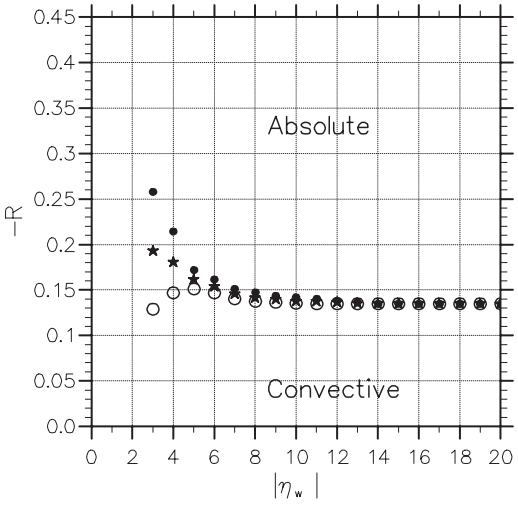

Figure 12. Wall effects on the CA transition for $\overline{M}_1 = 0$, $S = 1$ and $\theta = 0$: $-\eta_w$ moves (•); $+\eta_w$ moves (○); both walls move (⋆).

(Section 5.2.1) and more particularly to know if CA transition continuously evolves with η or if there are different modes which operate in the two considered configurations. Figure 13 shows the variation of the branch point parameters versus the similarity variable $|\eta_w|$ for different modes, for one Mach number, $\overline{M}_1 = 1.31$, with $\theta = 0°$ and $S = 1$.

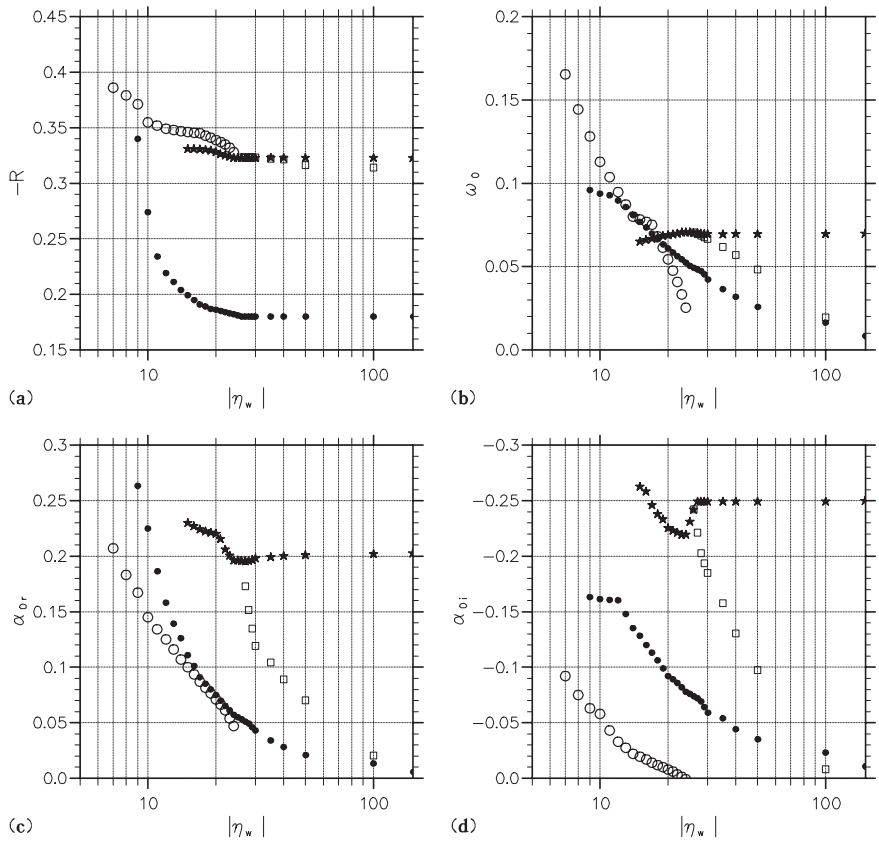

Figure 13. The CA transition boundary (a) and variation of the branch point parameters versus similarity variable η_w: (b) circular frequency ω_0; (c) wave-number α_{0_r}; (d) the spatial growth rate α_{0_i} for $\overline{M}_1 = 1.31$ for two-dimensional perturbation ($\theta = 0°$) and isothermal shear layer $S = 1$. Mode 1 (•), mode 2 (○), mode F (⋆) and mode I (□).

Modes 1 and 2 are those described in Section 5.2.1. For this Mach number value, the CA transition from mode 2 becomes dominant compared with that of mode 1. It is important to recall that mode 1 is no longer absolutely unstable when $\overline{M}_1 > 1.32$ (see Figure 8). For these two modes, their absolute spatial amplification rates $-\alpha_{0_i}$ and their absolute frequencies ω_0 strongly decrease when the wall distance increases. For $|\eta_w| > 24$, CA transition for mode 2 does not exist. As for mode 1, although $-R$ decreases when $|\eta_w|$ increases, its influence is almost negligible, $-\alpha_{0_i} < 10^{-3}$, when $|\eta_w| > 100$.

The mode represented in Figure 13 (here called mode "F") characterizes the CA transition for a free shear layer (see Section 5.1). This evolution is very different from those of modes 1 and 2. For $|\eta_w| > 30$, the variations of the branch parameters and the CA transition boundary are very weak. For $26 \leq |\eta_w| \leq 100$, another mode exists (called mode "I"), whose evolution is given in Figure 13. For $|\eta_w| \simeq 26$, with the precision of calculation, a pinching between three modes (one α_+ mode and two α_- modes) is observed. In fact, for $|\eta_w| > 26$, the "F" mode corresponds to a pinching between the α_+ and α_- modes and the "I" mode corresponds to a pinching between the same α_+ mode but another α_- mode. In these cases the pinching "F" and "I" occur for different branch parameters, but when $|\eta_w| \simeq 26$, the pinching "F" and "I" occur for the same branch parameters (same R, ω_0, α_0). Figure 14 shows the pinching between one α_+ branch and two α_- branches, when $|\eta_w| = 26$. When $|\eta_w| < 26$, the pinching "I" does not characterize the CA transition because it is a pinching between two α_- modes, while between $15 \leq |\eta_w| \leq 27$ the pinching "F" always characterizes the CA transition but in this zone the variation of the branch point parameters is high. For $|\eta_w| \leq 15$, the pinching "F" ceases to represent CA transition, because the pinching occurs for two α_- modes. Indeed, to determine if the pinching will occur between the α_+ mode and the α_- mode, it is necessary to recognize if the modes propagate in the positive or negative x-directions, i.e., to know if the generalized spatial branches are $\alpha_+(\omega)$ or $\alpha_-(\omega)$. The criterion to distinguish α_+ and α_- modes has been established by Briggs (1964). According to Briggs, in spatial instability modes of frequency ω_0, the calculation of the roots

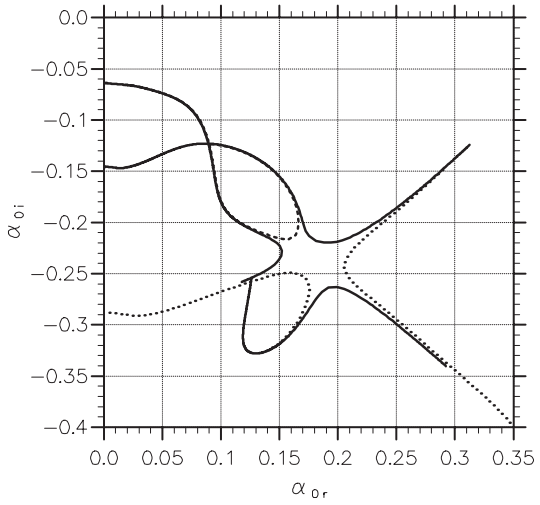

Figure 14. Locus of spatial branches as $\mathrm{Im}(\omega_0) = 0$, when $\eta_w = 26$, $S = 1$ and $\theta = 0°$ for $R = -0.321$ (——) and $R = -0.322$ (· · · · · ·).

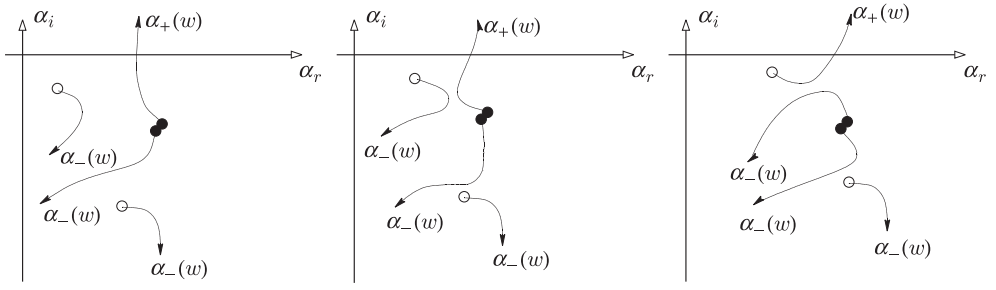

(a): For $\eta_w = 25$ to $\eta_w = 17$. (b): For $\eta_w = 16$ (b): For $\eta_w \leq 15$

Figure 15. Evolution of some eigenvalues around the pinching mode "F" (•) when $\mathrm{Re}(\omega) = \omega_0$ and $\mathrm{Im}(\omega)$ from 0 to $+\infty$. For $R = R_{\mathrm{CA}}$, $S = 1$, $\theta = 0°$ and for different values of η_w.

or poles of the dispersion relation $\mathcal{D}$ should start by setting the real part of ω equal to ω_0 and the imaginary part of ω to a large positive value. Zeros or poles of $\mathcal{D}$ lying in the upper half-α-plane represent modes propagating in the positive x-direction (i.e., an α_+ mode), while those in the lower half-α-plane represent waves propagating in the negative x-direction (i.e., α_- mode). Figure 15 shows the evolution of some eigenvalues around the pinching mode "F" for the large positive value of ω_i.

6. Conclusions

A detailed analysis of the CA nature of the instability of two-dimensional supersonic shear layers has been made. When the Mach number $\overline{M}_1 < 1$, for a given velocity ratio, the shear layer becomes more convectively unstable as the Mach number increases. This trend persists, for a fixed Mach number, as the low-speed side is heated relative to the high-speed side. On the other land, cooling the low-speed side extends the domain of absolute instability. In fact, for a sufficiently small temperature ratio (namely, $S < 0.1$), the shear layer may become absolutely unstable, even when the streams are very weak counterflowing. In the subsonic regime the most unstable instability wave is two-dimensional and the boundary between convective and absolute instability is thus determined by the pinching between two two-dimensional subsonic/subsonic modes. The effect of the parallel walls and the distance between them on the instability characteristics of the shear flow were investigated. The distance between such walls does not affect qualitatively the characteristics of the CA transition.

However, when the Mach number is supersonic, the effects of the walls are very important in CA transition. When the distance is decreased the reflections of the compression/expansion waves caused by the walls provide a feedback mechanism between the growing shear layer structure and the wave system. Moreover, when $\overline{M}_1 > 1$, multiple modes exist and the coalescence can occur between two α_+ modes as well as between α_+ and α_- modes.

When the walls are far enough ($\delta_w \ll \eta_w$), the boundary of the CA transition is determined by the pinching of the extension of the modes in the subsonic regime. According to Mach number $\overline{M}_1$, the angle of propagation of the disturbance θ and the temperature ratio S, this pinching mode is subsonic/subsonic, subsonic/supersonic or supersonic/supersonic. In all these cases the characteristics of the branch point parameters (ω_0, α_0) are quite different. When the walls are close to the shear layer, the transition curve for $\overline{M}_1$ between 0 and 1.0 and between 1.345 and 3.0 is defined by a single curve. However, for $\overline{M}_1$ between 1.0 and 1.345, multiple transition curves exist, due to the fact that multiple modes exist when $\overline{M}_1$ is greater than unity. In this region the mode that becomes absolutely unstable depends on the magnitude of the backflow. When $1 < \overline{M}_1 < 3$, for a confined shear flow, the CA transition with three-dimensional instability waves occurs for the amount of backflow greater than with two-dimensional instability waves. For a free shear layer the opposite trend is found. For a nonisothermal (free or confined) shear flow, the conclusions are identical with those presented for $\overline{M}_1 < 1$, the only evolution of the branch point parameters being highly dependent on η_w.

These results have particular relevance to the issue of the control of shear layers since injected disturbances can modify the streamwise evolution of a convectively unstable flow. Moreover, this analysis is a preliminary study for the characterization of CA transition in separated supersonic boundary layers. As a separated boundary layer behaves like a shear layer with a counterflow and with a wall on the low-speed side, knowledge of the CA transition in such shear layers is a useful guide to evaluate the CA transition in separated boundary layers. Indeed, we have shown that for a supersonic shear layer to develop an absolute instability, it is necessary either to cool the lower side of the shear layer or that $-R > 0.3$. In a realistic supersonic separated boundary layer, the intensity of the backflow does not exceed 15% of the external flow. It seems reasonable to think that the instabilities developing in a separated supersonic boundary layer are linearly convectively unstable. Finally, this analysis can undoubtedly apply in the industrial case of a wall cooled by a cold cooling film, for example, for the hot nozzle flow.

Acknowledgments

The authors thank the French Centre National d'Études Spatiales (CNES) and the Office National d'Étude et de Recherche Aérospatiale (ONERA-Toulouse) for respectively financial and technical support. The authors thank Dr. D. Arnal of the ONERA Toulouse for many helpful comments.

References

Blumen, W., Drazin, P.G., and Billings, D.F. (1975). Shear layer instability of an inviscid compressible fluid. Part 2. *J. Fluid Mech.*, **71**, 305–316.

Bridges, T.J., and Morris, P.J. (1984). Differential eigenvalue problems in which the parameter appears nonlinearly. *J. Comp. Phys.*, **55**, 437–460.

Briggs., R.J. (1964). *Electron-Stream Interaction with Plasmas*. MIT Press, Cambridge, Mass.

Dunn, D.W., and Lin, C.C. (1955). On the stability of the laminar bounary in a compressible fluid. *J. Aero. Sci.*, **22**, 455–477.

Gathmann, R.J., Si-Ameur, M., and Mathey, F. (1993). Numerical simulation of three-dimensional natural transition in thecompressible confined shear layer. *Phys. Fluids A*, **5**(11), 2946–2968.

Greenough, J.A., Riley, J.J., Soestrino M., and Eberhardt D.S. (1989). The effects of walls on a compresible mixing layer. AIAA Paper 89–0372.

Huerre, P., and Monkewitz, P. (1985). Absolute and convective instabilities in free shear layers. *J. Fluid Mech.*,. **159**, 151–168.

Jackson, T.L., and Grosch, C.E. (1989). Inviscid spatial stability of a compressible mixing layer. *J. Fluid Mech.*, **208**, 609–637.

Jackson, T.L., and Grosch, C.E. (1990a). Inviscid spatial stability of a compressible mixing layer. Part 2. The flame sheet model. *J. Fluid Mech.*, **217**, 391–420.

Jackson, T.L., and Grosch, C.E. (1990b). Absolute/convective instabilites and the convective Mach number in a compressible mixing layer. *Phys. Fluids A.* **2**(6), 949–955.

Jackson, T.L., and Grosch, C.E. (1991a). Inviscid spatial stability of a compressible mixing layer. Part 3. Effect of thermodynamics. *J. Fluid Mech.*, **224**, 159–175.

Jackson, T.L., and Grosch, C.E. (1991b). Inviscid spatial stability of a three-dimensional compressible mixing layer. *J. Fluid Mech.*, **231**, 35–50.

Lee, L., and Lin, C.C. (1946). Investigation of the stability of the laminar boundary layer in a compressible fluid. NACA TN 1115.

Lessen, L., Fox, J.A., and Zien, H.M. (1965). On the stability of the laminar mixing of two parallel streams of a compressible fluid. *J. Fluid Mech.*, **23**, 355–367.

Lessen, L., Fox, J.A., and Zien, H.M. (1966). Stability of the laminar mixing of two parallel streams with respect to supersonic disturbances. *J. Fluid Mech.*, **25**, 737–742.

Lock., R.C. (1951). The velocity distribution in the laminar boundary layer between parallel streams. Quart. *J. Mech. Appl. Math.* **4**, 42–63.

Mack, L. (1989). On the inviscid acoustic-mode instability of supersonic shear flows. *Proceeding of the Fourth Symposium on Numerical and Physical Aspects of Aerodynamics Flows*, pp. 1–15. California State University, Long Beach, CA.

Malik. M.R., Zang, T.A., and Hussaini, M.Y. (1985). A spectral collocation method for the Navier-Stokes equations. *J. Comp. Phys.*, **61**, 64–88.

Malik., M.R. (1990). Numerical methods for hypersonic boundary layer stability. *J. Comp. Phys.*, **86**, 376–413.

Pavithran, S., and Redekopp, L.G. (1989). The CA transition in subsonic mixing layers. *Phys. Fluids A*, **1**(10), 1736–1739.

Peroomian, O., and Kelly, R.E. (1994). Absolute and convective instabilites in a compressible confined mixing layer. *Phys. Fluids*, **6**(9), 3192–3194.

Tam, C.K.W., and Hu, F.Q. (1989). The instability and acoustic wave modes of supersonic mixing layers inside a rectangular channel. *J. Fluid Mech.*, **203**, 51–76.

Tam, C.K.W., and Morris, P.J. (1980). The radiation of sound by the instability waves of a compressible plane turbulent shear layer. *J. Fluid Mech.*, **98**, 349–381.

Zhuang, M., Dimotakis, P.E., and Kubota, T. (1989). The effect of walls on a spatially growing supersonic shear layer. *Phys. Fluids A*, **2**(4), 599–604.